# A novel hybrid finite element analysis of inplane singular elastic field around inclusion corners in elastic media

Meng-Cheng Chen *, Xue-Cheng Ping

*School of Civil Engineering, East China Jiaotong University, Shuang Gang Road, Jiangxi, Nanchang 330013, People's Republic of China*

ABSTRACT

This paper deals with the inplane singular elastic field problems of inclusion corners in elastic media by an *ad hoc* hybrid-stress finite element method. A one-dimensional finite element method-based eigenanalysis is first applied to determine the order of singularity and the angular dependence of the stress and displacement field, which reflects elastic behavior around an inclusion corner. These numerical eigensolutions are subsequently used to develop a super element that simulates the elastic behavior around the inclusion corner. The super element is finally incorporated with standard four-node hybrid-stress elements to constitute an *ad hoc* hybrid-stress finite element method for the analysis of local singular stress fields arising from inclusion corners. The singular stress field is expressed by generalized stress intensity factors defined at the inclusion corner. The *ad hoc* finite element method is used to investigate the problem of a single rectangular or diamond inclusion in isotropic materials under longitudinal tension. Comparison with available numerical results shows the present method is an efficient mesh reducer and yields accurate stress distribution in the near-field region. As applications, the present *ad hoc* finite element method is extended to discuss the inplane singular elastic field problems of a single rectangular or diamond inclusion in anisotropic materials and of two interacting rectangular inclusions in isotropic materials. In the numerical analysis, the generalized stress intensity factors at the inclusion corner are systematically calculated for various material type, stiffness ratio, shape and spacing position of one or two inclusions in a plate subjected to tension and shear loadings.

© 2008 Elsevier Ltd. All rights reserved.

## 1. Introduction

Much attention has been paid to inclusion problems by many researchers since the first solution to the ellipsoidal inclusion problems by Eshelby (Eshelby, 1957). The application background is found in microstructures, composite material structures and others (Mura, 1987; Nemat-Nasser and Muneo, 1999; Buryachenko, 2007).

To solve elastic inclusion problems, both the analytical and numerical methods were applied. Among the works on analytical solution, the representative ones that should be mentioned are those of Eshelby (1957), Kröner (1958), Hill (1965), Budiansky (1965), Mori and Tanaka (1973) as well as Kushch et al. (2005). However, these analytical solutions are either limited to very simple geometries such as ellipsoidal inclusions or require high level of mathematical competence. Therefore, most engineering problems of ellipsoidal or irregular shaped inclusions have to resort to numerical methods such as the finite element method (FEM), the volume integral equation method (VIEM), the boundary integral equation method (BIEM) and others.

---

* Corresponding author. Tel./fax: +086 791 7046552.
  *E-mail address:* chenmch@ecjtu.jx.cn (M.-C. Chen).

The conventional FEM has been used to solve various kinds of inclusions (Ghosh and Mukhopadhyay, 1993; Nakamura and Suresh, 1993 as well as Thomson and Hancock, 1984). However, due to the need for domain discretization, a lot of finite elements must be used for more accurate numerical results. The VIEM is an effective method for the analysis of the inclusions embedded in an isotropic matrix or for coating problems (Buryachenko and Bechel, 2000; Dong and Bonnet, 2002; Dong et al., 2002; Lee et al., 2001 and Nakasone et al., 2000). Compared with the conventional FEM, the VIEM only discretizes the inclusion parts. However, it is difficult to extend this approach to the anisotropic medium due to the use of complex fundamental solutions. Relative to the conventional FEM and VIEM, the BIEM is a more efficient and accurate one for solving inclusion problems. It has been successfully applied for the solution of inclusion problems of various shapes (Tan et al., 1992; Chen and Nisitani, 1993; Chen, 1994; Noda et al., 2000; Dong et al., 2003). However, the method also needs the fundamental solution, which is not easy-to-obtain or impossible-to-obtain for composite materials; and the boundary integral equation must be formulated for each inclusion, which might be inconvenient for solving problems containing many inclusions of irregular shapes. In comparison with the BIEM in the accuracy of numerical solutions, the hybrid-stress finite element method developed more than 40 years ago by Pian (1964) is now well recognized as a powerful and easy-to-use tool for solving a variety of two-dimensional linear elasticity problems containing a single or multiple singular points (Tong et al., 1973; Tong, 1977; Moriya, 1984; Lee and Gao, 1995; Zhang and Katusbe, 1995, 1997; Wang et al., 2004 and the authors, 2001a, 2001b, 2007a, 2007b, 2008). This makes the method attractive and potentially very useful in micromechanics of fibrous composites because it provides an efficient tool for analyzing the advanced one-inclusion or many-inclusion model problems with an accurate account for elastic behavior in the near-field region. In the numerical study of composite materials reinforced by circular inclusions, the method has been applied successfully only by Zhang and Katusbe (1995, 1997).

At the same time, to the best of the author's knowledge, the studies related to interacting non-ellipsoidal inclusions by the hybrid-stress finite element method are absent. Moreover, a numerical solution of even a single non-ellipsoidal inclusion by the hybrid-stress finite element method could not be found in the literature. This may result from a fact that constructing a super inclusion corner element needs the analytical solution of the singularity order and angular variation of singular elastic field that reflect local elastic behavior around the inclusion corner, whose derivation introduces formidable mathematical difficulties for most composite materials.

In the present work, a one-dimensional finite element formulation developed by Sze and Wang (2000), Sze et al. (2001) is first applied for the numerical solution of the order of stress singularities and the angular variation of stress and displacements fields. These numerical fields are subsequently used to develop a super element that simulates the elastic behavior around an inclusion corner. The super element is finally incorporated with standard four-node hybrid-stress elements to constitute an *ad hoc* hybrid-stress finite element method for the analysis of local singular stress fields arising from inclusion corners. To compare the available reference solutions, the *ad hoc* finite element method is used to solve the problem of a single rectangular or diamond inclusion in isotropic materials under longitudinal tension. To present its applicability, the present *ad hoc* finite element method is extended to discuss the inplane singular elastic field problems of a single rectangular inclusion in an anisotropic plate and of two interacting rectangular inclusions in an isotropic plate. In the numerical analysis, the generalized stress intensity factors at the inclusion corner are systematically calculated for various material types, stiffness ratio, shape and spacing position of one and two inclusions in a plate subjected to tension and shear loadings.

## 2. Expressions for total elastic fields around an inclusion corner

Consider an infinite plate containing an irregular-shaped inclusion, as shown in Fig. 1. The singular stress field around the inclusion corner is analyzed. It is convenient to use a local coordinate system centered at the corner to analyze the local elastic behavior. Fig. 2 shows the local configuration around the corner o. In Fig. 2, two dissimilar wedges with subtending angles of $\alpha$ and $\alpha_1 + \alpha_2$ ($\alpha + \alpha_1 + \alpha_2 = 2\pi$), respectively, are bonded perfectly along both of their interfaces. Each of which may be made of an isotropic, anisotropic, piezoelectric or else material. Wedge 1 is occupied by domain $\Omega^1$, and wedge 2 by domain $\Omega^2$. Let $(r, \theta)$ be a local polar coordinate system centered at the corner o, so that the axis of $\theta = 0$ is the bisector of the two wedges. Therefore, when setting $\theta = 0$, we have $\alpha_1 = \alpha_2$. The stress and displacement field near the corner is evaluated by using a one-dimensional eigenanalysis finite element formulation. The formulation is straightforward as will be shown herein.
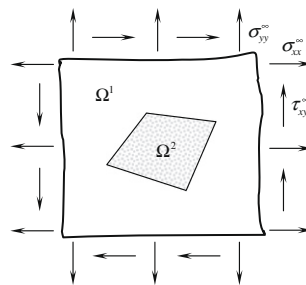


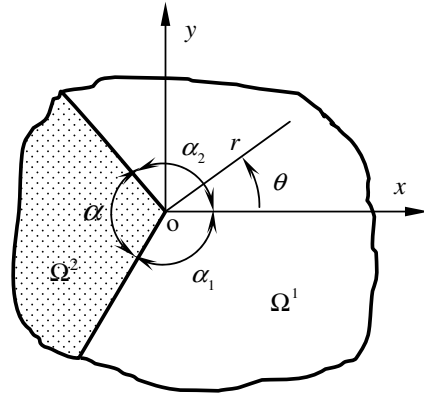**Fig. 1.** An infinite plate containing a non-ellipsoidal inclusion.

**Fig. 2.** Local coordinate system near the inclusion corner.

According to previous studies (Sze and Wang, 2000; the authors, 2001a and 2001b), the following one-dimensional finite element characteristic formulation on stress singularities around the corner is given as:

$$\sum_{e^1+e^2} [(\delta\mathbf{q}^e)^T(\lambda^2\widetilde{\mathbf{P}}^e + \lambda\widetilde{\mathbf{Q}}^e + \widetilde{\mathbf{R}}^e)\mathbf{q}^e] = \mathbf{0} \tag{1}$$

in which $\sum_{e^1+e^2}$ represents the assemblage of elements belonging to wedge domain 1 and 2; $\lambda$ are eigenvalues (called as stress singularity orders as well); $\mathbf{q}^e$ are eigenvectors or generalized nodal displacement components in the element "$e$"; the element matrices $\widetilde{\mathbf{P}}^e, \widetilde{\mathbf{Q}}^e$ and $\bar{\mathbf{P}}^e$ are defined in Sze and Wang (2000) as well as the authors (2001a and 2001b). Eq. (1) can be transformed into a standard characteristic equation by proper manipulations, and then eigenvalues $\lambda$ and eigenvectors $\mathbf{q}^e$ are solved from the equation with standard numerical subroutines. The element matrices $\widetilde{\mathbf{P}}^e, \widetilde{\mathbf{Q}}^e$ and $\bar{\mathbf{P}}^e$ are evaluated using numerical integration by means of Gaussian quadrature for isotropic materials. However, for anisotropic materials whose properties are angular functions, the matrices must be transformed at each Gauss point during the numerical evaluation of the integrals, so that the anisotropic in the material is correctly taken into consideration.

When either one of domain $\Omega^1$ or domain $\Omega^2$ or both are polarized piezoelectric materials, some modifications to one-dimensional eigenanalysis finite element formulation (1) should correspondingly be made due to the additional piezoelectric effect. To save space, we are not going to discuss how the eigenanalysis finite element formulation of piezoelectric materials is modified herein. The interested readers can refer to Sze et al. (2001) and our previous publications (2006, 2007a, 2007b) for more details.

By using the numerical solutions of singularity orders $\lambda_n$ and generalized nodal displacement components $\mathbf{q}^{e(n)}$ from Eq. (1), the general expressions of total asymptotic displacements $\mathbf{u}(r, \theta)$ and stresses $\boldsymbol{\sigma}(r,\theta)$ around the inclusion corner in elastic materials are written as

$$\mathbf{u}(r,\theta) = \sum_{n=1}^{N+M} \beta^{(n)} r^{\lambda_n+1}\overline{\mathbf{U}}^{(n)}(\theta) = \sum_{n=1}^{N} (\beta_R^{(n)}\mathbf{U}_R^{(n)}(r,\theta) + \beta_I^{(n)}\mathbf{U}_I^{(n)}(r,\theta)) + \sum_{n=1}^{M} \beta^{(n)}\mathbf{U}^{(n)}(r,\theta) = \mathbf{U}(r,\theta)\boldsymbol{\beta} \tag{2}$$

$$\boldsymbol{\sigma}(r,\theta) = \sum_{n=1}^{N+M} \beta^{(n)} r^{\lambda_n}\bar{\boldsymbol{\sigma}}^{(n)}(\theta) = \sum_{n=1}^{N} (\beta_R^{(n)}\boldsymbol{\Sigma}_R^{(n)}(r,\theta) + \beta_I^{(n)}\boldsymbol{\Sigma}_I^{(n)}(r,\theta)) + \sum_{n=1}^{M} \beta^{(n)}\boldsymbol{\Sigma}^{(n)}(r,\theta) = \boldsymbol{\Sigma}(r,\theta)\boldsymbol{\beta} \tag{3}$$

where subscripts R and I indicates the real part and imaginary part of a complex variable, respectively and $i = \sqrt{-1}$; $\boldsymbol{\beta}$ are unknown coefficients to be determined, i.e., $\boldsymbol{\beta} = [\beta_R^{(1)}\beta_I^{(1)}\cdots\beta_R^{(N)}\beta_I^{(N)}\beta^{(1)}\cdots\beta^{(M)}]^T$; the quantity with subscript **P** is an interim one in the polar coordinate system; and $N$ represents the number of complex singularity order $\lambda_n$ truncated and $M$ the number of real singularity order $\lambda_n$ truncated. Moreover, in Eq. (1), it has been arranged as $\lambda_n \leqslant \lambda_{n+1}$ (herein equal means multiple roots), and in the scope of fracture mechanics, $Re(\lambda) < -1$ should be excluded in the series. $\mathbf{U}^{(n)}(r,\theta),\boldsymbol{\Sigma}^{(n)}(r,\theta)$ and $\mathbf{U}_l^{(n)}(r,\theta)$, $\boldsymbol{\Sigma}_l^{(n)}(r,\theta)(l = R, I)$ can be respectively computed from the non-dimensional angular distributions of $\overline{\mathbf{U}}^{(n)}(\theta)$ and $\bar{\boldsymbol{\sigma}}^{(n)}(\theta)$ which are obtained from the singularity orders $\lambda_n$ and the eigenvectors $\mathbf{q}^{e(n)}$.

## 3. Super inclusion corner element stiffness matrix

Sound variational basis and high coarse mesh accuracy of super crack-tip and wedge-tip hybrid elements for conventional materials have been discussed (Tong et al., 1973 and the authors, 2001b). Similarly, to formulate finite element calculations for the singular elastic fields around an inclusion corner in elastic materials, a super $n$-sided polygonal inclusion corner element embedded with a part of an inclusion corner, as shown in Fig. 3(a), will be developed based on Eqs. (2) and (3).

Our goal is to establish the relationship between the element's nodal force and displacement, or simply, to formulate the element stiffness matrix. The key idea in formulating this *ad hoc* element is to decompose the original problem (Fig. 3(a)) into

two boundary value problems as shown in Fig. 3(b) and (c): (1) a specified mixed boundary value problem in the matrix domain $\Omega^1$ with boundaries $C^1, \Gamma_1$ and $\Gamma_2$; (2) a specified mixed boundary value problem in the non-ellipsoidal inclusion domain $\Omega^2$ with boundaries $C^2$, $\Gamma_1$ and $\Gamma_2$. $C^1$ and $C^2$ are the element's outer boundary with neighboring elements, and $\Gamma_1$ and $\Gamma_2$ are inner interface between the matrix and the inclusion. Following the Hellinger-Reissner principle as well as Zhang and Katsube's work (1995), similarly, we define the following two separate hybrid functionals for these two problems:

*For problem* 1

$$\pi_m^e = \int_{\Omega^1} \left( \frac{1}{2} \boldsymbol{\sigma}_m^T \mathbf{S}_m \boldsymbol{\sigma}_m - \boldsymbol{\sigma}_m^T \mathbf{D} \mathbf{u}_m \right) d\Omega - \int_{C^1} \mathbf{t}_m^T (\tilde{\mathbf{u}}^{(1)} - \mathbf{u}_m) dS + \int_{\Gamma_1 + \Gamma_2} (\tilde{\mathbf{t}}^{(1)})^T \mathbf{u}_m dS \tag{4}$$

*For problem* 2

$$\pi_I^e = \int_{\Omega^2} \left( \frac{1}{2} \boldsymbol{\sigma}_I^T \mathbf{S}_I \boldsymbol{\sigma}_I - \boldsymbol{\sigma}_I^T \mathbf{D} \mathbf{u}_I \right) d\Omega - \int_{C^2} \mathbf{t}_I^T (\tilde{\mathbf{u}}^{(2)} - \mathbf{u}_I) dS + \int_{\Gamma_1 + \Gamma_2} (\tilde{\mathbf{t}}^{(2)})^T \mathbf{u}_I dS \tag{5}$$

where $\mathbf{u}, \boldsymbol{\sigma}, \mathbf{t}$ and $\mathbf{S}$ are, respectively, the stress, displacement, boundary traction vectors and the elastic compliance matrix; $\mathbf{D}$ is the matrix differential operator relating strains to displacements; and the symbol $\sim$ represents a specified quantity. Based on the hybrid-stress finite element method (Pian, 1964), the boundary displacements $\tilde{\mathbf{u}}^{(1)}$ and $\tilde{\mathbf{u}}^{(2)}$ are assumed separately from $\mathbf{u}$ and are expressed in terms of the displacements of the element. The boundary tractions $\tilde{\mathbf{t}}^{(1)}$ and $\tilde{\mathbf{t}}^{(2)}$ are assumed to be specified and are actually unknown.

The stationary values of the two functionals defined by Eqs. (4) and (5) yield the following two sets of equations:

*For problem* 1

$$\mathbf{D}^T \boldsymbol{\sigma}_m = 0, \quad \mathbf{S}_m \boldsymbol{\sigma}_m = \mathbf{D} \mathbf{u}_m \text{ in } \Omega^1 \tag{6}$$

$$\mathbf{t}_m = \mathbf{n}^{(1)} \boldsymbol{\sigma}_m \text{ on } C^1, \quad \Gamma_1 \text{ and } \Gamma_2 \tag{7}$$

$$\mathbf{u} = \tilde{\mathbf{u}}^{(1)} \text{ on } C^1, \quad \mathbf{t} = \tilde{\mathbf{t}}^{(1)} \text{ on } \Gamma_1 \text{ and } \Gamma_2 \tag{8}$$

*For problem* 2

$$\mathbf{D}^T \boldsymbol{\sigma}_I = 0, \quad \mathbf{S}_I \boldsymbol{\sigma}_I = \mathbf{D} \mathbf{u}_I \text{ in } \Omega^2 \tag{9}$$

$$\mathbf{t}_I = \mathbf{n}^{(2)} \boldsymbol{\sigma}_I \text{ on } C^2, \quad \Gamma_1 \text{ and } \Gamma_2 \tag{10}$$

$$\mathbf{u} = \tilde{\mathbf{u}}^{(2)} \text{ on } C^2, \quad \mathbf{t} = \tilde{\mathbf{t}}^{(2)} \text{ on } \Gamma_1 \text{ and } \Gamma_2 \tag{11}$$

in which $\mathbf{n}^{(i)}$ is a $2 \times 3$ matrix of the unit normal to boundary $C^{(i)}$ and $\Gamma_{(i)}$. It is seen from the above equations that the true solutions of the two problems minimize the hybrid functionals. We may simplify the functional by constructing the stress $\boldsymbol{\sigma}$ and displacement $\mathbf{u}$ fields in such a manner that Eqs. (6), (7), (9) and (10) are automatically satisfied. By doing this and using the divergence theorem over $\Omega^1$ and $\Omega^2$, the two functionals are reduced to

$$\pi_m^e = \frac{1}{2} \int_{C^1} \mathbf{t}_m^T \mathbf{u}_m dS - \int_{C^1} \mathbf{t}_m^T \tilde{\mathbf{u}}^{(1)} dS + \int_{\Gamma_1 + \Gamma_2} (\tilde{\mathbf{t}}^{(1)})^T \mathbf{u}_m dS - \frac{1}{2} \int_{\Gamma_1 + \Gamma_2} \mathbf{t}_m^T \mathbf{u}_m dS \tag{12}$$

$$\pi_I^e = \frac{1}{2} \int_{C^2} \mathbf{t}_I^T \mathbf{u}_I dS - \int_{C^2} \mathbf{t}_I^T \tilde{\mathbf{u}}^{(2)} dS + \int_{\Gamma_1 + \Gamma_2} (\tilde{\mathbf{t}}^{(2)})^T \mathbf{u}_I dS - \frac{1}{2} \int_{\Gamma_1 + \Gamma_2} \mathbf{t}_I^T \mathbf{u}_I dS \tag{13}$$

In order to recover the solution for the original problem from those of two decomposed problems, the traction reciprocity $\mathbf{t}$ conditions and the displacement $\mathbf{u}$ compatibility conditions are necessary to be imposed:
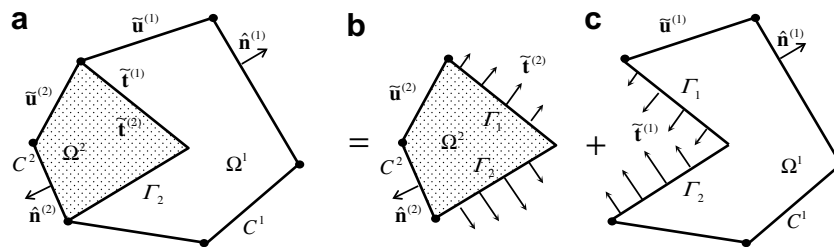


**Fig. 3.** Element decomposition: (a) original element; (b) inclusion domain with mixed boundary values; (c) matrix domain with mixed boundary values.

$$\mathbf{u}_{\mathrm{I}} = \mathbf{u}_{\mathrm{m}} \text{ on } \Gamma_1 \text{ and } \Gamma_2 \tag{14}$$

$$\mathbf{t}^{(1)} = -\mathbf{t}^{(2)}, \quad \mathbf{t}_{\mathrm{m}} = -\mathbf{t}_{\mathrm{I}} \text{ on } \Gamma_1 \text{ and } \Gamma_2 \tag{15}$$

The functional $\pi^e$ for the original problem is rewritten as $\pi^e = \pi_{\mathrm{m}}^e + \pi_{\mathrm{I}}^e$. Therefore, adding Eqs. (12) and (13), and noting conditions (14) and (15), we have

$$\pi^e = \frac{1}{2} \int_{C^1} \mathbf{t}_{\mathrm{m}}^{\mathrm{T}} \mathbf{u}_{\mathrm{m}} dS + \frac{1}{2} \int_{C^2} \mathbf{t}_{\mathrm{I}}^{\mathrm{T}} \mathbf{u}_{\mathrm{I}} dS - \int_{C^1} \mathbf{t}_{\mathrm{m}}^{\mathrm{T}} \tilde{\mathbf{u}}^{(1)} dS - \int_{C^2} \mathbf{t}_{\mathrm{I}}^{\mathrm{T}} \tilde{\mathbf{u}}^{(2)} dS \tag{16}$$

If we write $\mathbf{t}_{\mathrm{m}}$ and $\mathbf{t}_{\mathrm{I}}$ as $\mathbf{t}$, $\mathbf{u}_{\mathrm{m}}$ and $\mathbf{u}_{\mathrm{I}}$ as $\mathbf{u}$, and $\tilde{\mathbf{u}}^{(1)}$ and $\tilde{\mathbf{u}}^{(2)}$ as $\tilde{\mathbf{u}}$, Eq. (16) is rewritten as

$$\pi^e = \frac{1}{2} \int_C \mathbf{t}^{\mathrm{T}} \mathbf{u} dS - \int_C \mathbf{t}^{\mathrm{T}} \tilde{\mathbf{u}} dS \tag{17}$$

where $C = C^{(1)} + C^{(2)}$. Note the integrands $\mathbf{u}$ and $\mathbf{t} = \mathbf{n}\boldsymbol{\sigma}$ of Eq. (23) are integrated in the Cartesian coordinate system, which should be obtained from $\mathbf{u}(r, \theta)$ and $\boldsymbol{\sigma}(r, \theta)$ in the polar coordinate system given in Eqs. (2) and (3).

Using Eqs. (2), (3) and (17), we have the following stiffness matrix of the super inclusion corner element:

$$\mathbf{K}_{S-I} = \mathbf{G}^{\mathrm{T}} \mathbf{H}^{-1} \mathbf{G} \tag{18}$$

where $\mathbf{G}$ and $\mathbf{H}$ are one-dimensional integrals along the boundaries of the super inclusion corner element as shown in Fig. 4, namely:

$$\mathbf{H} = \frac{1}{2} \int_C [(\mathbf{n}\Sigma(x,y))^T \mathbf{U}(x,y) + (\mathbf{U}(x,y))^T (\mathbf{n}\Sigma(x,y))] dS, \quad \mathbf{G} = \int_C (\mathbf{n}\Sigma(x,y))^T \mathbf{L} dS$$

$$\mathbf{L} = \left[ \left(1 - \frac{s}{l}\right) \mathbf{I}_2 \quad \frac{s}{l} \mathbf{I}_2 \right]$$

in which $s$ is the distance measured from a point $p$ on the integration boundary segment to the first node of integration boundary segment as shown in Fig. 4, and $l$ is the length between two nodes of the integration boundary segment; $\mathbf{I}_2$ is the second order identity matrix.

This *ad hoc* element is used to model the near-field region and is in conjunction with the conventional four-node hybrid-stress elements in the far-field region for the analysis of displacement and stress fields in the entire region, thus finally singular stress fields around the inclusion corner are obtained.

## 4. Definition of generalized stress intensity factor (GSIF)

### 4.1. GSIF around an inclusion corner in isotropic materials

As for the problem of non-ellipsoidal inclusions in isotropic materials, Chen and Nisitani (1993) and Chen (1994) used the complex function approach and the body force method to study it. According to their studies, the singular stress field around the inclusion corner can be expressed, in a simple form, as a sum of two items: one written in a form of $r^{\lambda_1}$ is corresponding to the mode I deformation and the other written in a form of $r^{\lambda_2}$ the mode II deformation. The stress fields due to the mode I and II deformations are symmetric and skew-symmetric with respect to the axis of $\theta = 0$ (see Fig. 2), respectively. The orders of stress singularity for the mode I and II, $\lambda_1$ and $\lambda_2$, are generally different, and determined from Eq. (1), respectively and arranged as $\lambda_2 \leqslant \lambda_1$. Therefore, when singular stresses at every $\theta$ are calculated from Eq. (3), For example, at points on the axis $\theta = 0$, the singular stresses $\sigma_{\theta\theta}$ for the mode I and $\sigma_{r\theta}$ for the mode II are related with the values of generalized stress intensity factors $K_{\mathrm{I},\lambda_1}$ and $K_{\mathrm{II},\lambda_2}$, respectively, as follows:


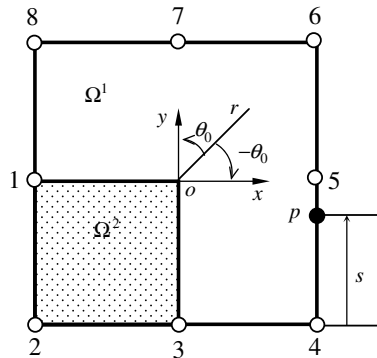
Fig. 4. Configuration of a multiple-node super inclusion corner element.

$$K_{I,\lambda_1} = \frac{1}{f_{\theta\theta,1}^I(0)} \lim_{r \to 0} \sqrt{2} r^{-\lambda_1} \sigma_{\theta\theta}(r, \theta = 0) \tag{19}$$

$$K_{II,\lambda_2} = \frac{1}{f_{r\theta,1}^{II}(0)} \lim_{r \to 0} \sqrt{2} r^{-\lambda_2} \sigma_{r\theta}(r, \theta = 0) \tag{20}$$

in which the angular functions $f_{\theta\theta,1}^I(0)$ and $f_{r\theta,1}^{II}(0)$ are given by Chen (1994).

### 4.2. GSIF around an inclusion corner in anisotropic materials

With regard to the problem of non-ellipsoidal inclusions in anisotropic materials, if the bisector of the two wedges is alien with x-axis (see Fig. 2) and the principal axis of material is consistent with the coordinate axis, the distribution of singular stress filed, like that in isotropic materials, is symmetric and skew-symmetric with respect to the axis of $\theta = 0$. The generalized stress intensity factor (GSIF) can be still computed from Eqs. (19) and (20). Otherwise, the distributions of singular stress fields around an inclusion corner in anisotropic materials are very complicated and the formulations aforementioned cannot be used. Under prerequisites for convenience in use and safety in components, the strongest singularity and the stresses on the interface are usually used to define the generalized stress intensity factor (GSIF), namely:

$$K_1 = \lim_{r \to 0} \sqrt{2} r^{-\lambda_1} \sigma_{\theta\theta}(r, \theta_0), \quad K_2 = \lim_{r \to 0} \sqrt{2} r^{-\lambda_1} \sigma_{r\theta}(r, \theta_0) \tag{21}$$

where $\lambda_1$ is the order of dominant singularity and $\theta_0$ is the angle between the interface and the bisector as shown in Fig. 4.

## 5. Application

A number of numerical examples are considered to demonstrate the efficacy of the present *ad hoc* hybrid-stress finite element technique in this section. Some of them have been discussed in the previous studies (Chen, 1994; Chen and Nisitani, 1993), and the others are new.

### 5.1. Material property

Several kinds of materials such as isotropic materials, anisotropic materials and piezoelectric materials are used in the present numerical study. The relevant non-zero materials parameters with respect to their principal material directions 1, 2 and 3 (also poling direction for piezoelectric materials) are given below:

(1) Isotropic material

**Pb** $E = 17 \times 10^3$ N/mm$^2$, $\upsilon = 0.42$

**Al** $E = 68.9 \times 10^3$ N/mm$^2$, $\upsilon = 0.25$

**Cu** $E = 129.8 \times 10^3$ N/mm$^2$, $\upsilon = 0.343$

**Ni** $E = 210 \times 10^3$ N/mm$^2$, $\upsilon = 0.31$

(2) Ceramic material
**Al$_2$O$_3$**: $E = 359 \times 10^3$ N/mm$^2$, $\upsilon = 0.20$

(3) High modulus epoxy-matrix composite

$E_1 = 137.9, E_2 = 14.48, E_3 = 14.48, \mu_{12} = 4.98 \times 10^3$ N/mm$^2$,
$\upsilon_{12} = 0.21, \upsilon_{21} = 0.022, \upsilon_{32} = 0.21$

(4) Piezoelectric material
**PZT5H**:
$c_{11} = 126.0, c_{12} = 55.0, c_{13} = 53.0, c_{33} = 117.0, c_{44} = 35.3 \times 10^3$ N/mm$^2$;
$e_{15} = 23.3, e_{31} = -6.5, e_{33} = 17.0 \times 10^6$ pC/mm$^2$;
$\kappa_{11} = 15100.0, \kappa_{33} = 13000.0 \times 10^6$ pC/Nmm$^2$

### 5.2. Benchmark example

As shown in Fig. 5(a) and (b), an infinite plate containing a single rectangular or diamond inclusion under remote loading is used as benchmark examples to validate the present method to be effective and applicable. Suppose that domain $\Omega^1$ is occupied by an isotropic material with elastic constants $(\mu_1, \upsilon_1)$, and domain $\Omega^2$ by an isotropic material with elastic constants $(\mu_2, \upsilon_2)$. For the sake of comparison, the dimensionless stress intensity factors $F_{I, \lambda_1}$ and $F_{II, \lambda_2}$ are used as:

*For a rectangular inclusion*

$$F_{\mathrm{I},\lambda_1} = \frac{K_{\mathrm{I},\lambda_1}}{\sigma_{yy}^{\infty} b^{-\lambda_1}}, \quad F_{\mathrm{II},\lambda_2} = \frac{K_{\mathrm{II},\lambda_2}}{\tau_{xy}^{\infty} b^{-\lambda_2}} \tag{22}$$

*For a diamond inclusion*

$$F_{\mathrm{I},\lambda_1} = \frac{K_{\mathrm{I},\lambda_1}}{\sigma_{yy}^{\infty} l^{-\lambda_1}}, \quad F_{\mathrm{II},\lambda_2} = \frac{K_{\mathrm{II},\lambda_2}}{\tau_{xy}^{\infty} l^{-\lambda_2}} \tag{23}$$

x in which $b$ is half the width of the rectangular inclusion and $l$ half the width of the diamond inclusion (see Fig. 5); $\sigma_{yy}^{\infty}$ and $\tau_{xy}^{\infty}$ are tension load and shear load, respectively.

### 5.2.1. Convergence of numerical results

In this part, to discuss the effects of the size of the super inclusion corner element on the numerical results, an infinite plate containning an isotropic square inclusion ($b = l$) in isotropic materials under remote loading is considered, as shown in Fig. 5(a). The plane stress condition is assumed. Their comparisons are respectively given in Tables 1 and 2. Table 1 is corresponding to the dimensionless stress intensity factors $F_{\mathrm{I},\lambda_1}$ and $F_{\mathrm{II},\lambda_2}$ for a square inclusion with different stiffness ratios of materials under tension loading $\sigma_{yy}^{\infty}$, and Table 2 under shear loading $\tau_{xy}^{\infty}$. Taking $\mu_2/\mu_1 = 10$ under tension loading $\sigma_{yy}^{\infty}$ as an example, the analytical solutions (Chen, 1994) of $F_{\mathrm{I},\lambda_1}$ and $F_{\mathrm{II},\lambda_2}$ are 0.2402 and −0.4876, respectively, and the present numerical results of $F_{\mathrm{I},\lambda_1}$ and $F_{\mathrm{II},\lambda_2}$ are, respectively, 0.1846 and −0.4737 at size 2.0b × 2.0b, and 0.2397 and −0.4860 at size 0.2b × 0.2b. It is seen that the discrepancies between the analytical solutions and the present numerical results are respectively −23.15% and −2.85% at size 2.0b × 2.0b, but −0.21% and −0.33% at size 0.2b × 0.2b. Therefore, we can draw a conclusion that the errors of numerical results decrease with decreasing the size of the inclusion corner element. In the numerical analysis, one super inclusion corner element and 285 four-node quadrilateral elements are used.

### 5.2.2. Comparisons with available solutions

As the first benchmark example, herein an infinite plate containing an isotropic rectangular inclusion in isotropic materials under only tension loading, shown in Fig. 5(a), is considered under the condition of plane stress. The singular stress fields around the inclusion corner A are analyzed. To simulate the infinite effect, the width and the height of the plate are set to be $w = 20b$ and $h = 10l$, respectively, in which $b$ and $l$ are respectively half the width and height of the inclusion. Due to the symmetry of the geometry and loading, only one-quarter of the geometry is needed for finite element mesh division. Configuration of mesh division around the rectangular inclusion corner is given in Fig. 6. To verify the present method, the
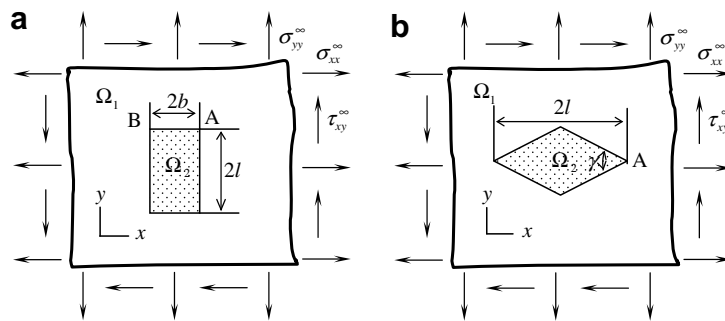


**Fig. 5.** Configuration of inclusions treated in the numerical examples.

**Table 1**
$F_{\mathrm{I},\lambda_1}$ and $F_{\mathrm{II},\lambda_2}$ for a square inclusion under uniaxial tension loading $\sigma_{yy}^{\infty}$

| Sizes (mm) | SIFs | $\mu_2/\mu_1$ | | | |
|---|---|---|---|---|---|
| | | 0.1 | 2 | 10 | 100 |
| 2.0b × 2.0b | $F_{\mathrm{I},\lambda_1}$ | 0.3875 | 0.2015 | 0.1846 | 0.2527 |
| | $F_{\mathrm{II},\lambda_2}$ | 2.4033 | −2.3271 | −0.4737 | −0.3675 |
| 1.0b × 1.0b | $F_{\mathrm{I},\lambda_1}$ | 0.3861 | 0.1988 | 0.2237 | 0.2530 |
| | $F_{\mathrm{II},\lambda_2}$ | 2.4549 | −2.3293 | −0.4795 | −0.3687 |
| 0.2b × 0.2b | $F_{\mathrm{I},\lambda_1}$ | 0.3837 | 0.1967 | 0.2397 | 0.2547 |
| | $F_{\mathrm{II},\lambda_2}$ | 2.4727 | −2.3462 | −0.4860 | −0.3546 |

**Table 2**
$F_{I,\lambda_1}$ and $F_{II,\lambda_2}$ for a square inclusion under shear loading $\tau_{xy}^\infty$

| Sizes (mm) | SIFs | $\mu_2/\mu_1$ | | | |
|---|---|---|---|---|---|
| | | 0.1 | 2 | 10 | 100 |
| $2.0b \times 2.0b$ | $F_{I,\lambda_1}$ | −11.7980 | 0.1516 | 0.6130 | 0.6673 |
| | $F_{II,\lambda_2}$ | −0.0005 | −0.0043 | 0.0043 | 0.0029 |
| $1.0b \times 1.0b$ | $F_{I,\lambda_1}$ | −11.8577 | 0.1528 | 0.6346 | 0.6525 |
| | $F_{II,\lambda_2}$ | −0.0016 | −0.0019 | −0.0004 | 0.0005 |
| $0.2b \times 0.2b$ | $F_{I,\lambda_1}$ | −11.7653 | 0.1524 | 0.6341 | 0.6319 |
| | $F_{II,\lambda_2}$ | −0.0021 | −0.0018 | −0.0010 | −0.0002 |

relationships between the dimensionless stress intensity factors $F_{I,\lambda_1}$ as well as $F_{II,\lambda_2}$ against $l/b$ is investigated again, and it can be seen from Fig. 7(a) and (b) that the present numerical results coincide with those of Chen (1994). In the numerical calculation, one super inclusion corner element and 285 four-node quadrilateral elements are employed.

As shown in Fig. 5(b), an infinite plate containing an isotropic diamond inclusion in isotropic materials only under tension loading is considered as the second benchmark example. The plane stress condition is assumed. The singular stress fields around the inclusion corner A are analyzed. To simulate the infinite effect, the width and the height of the plate are set to be $w = 40l$ and $h = 40l$, respectively, where $l$ is half the width of the diamond inclusion. Due to the symmetry of the geometry and loading, in the numerical calculations, only the right area of the geometry in Fig. 5(b), i.e., the right area of $40l \times 40l$, is needed for finite element mesh division. Diagram of the finite element mesh division is shown in Fig. 8. Table 3 describes the relationship between the dimensionless stress intensity factors $F_{I,\lambda_1}$ as well as $F_{II,\lambda_2}$ against the ratio of shear material constants $\mu_2/\mu_1$. We can see from Table 3 that the present numerical results are in good agreement with those of Chen (1994). The maximum error is less than 2.91%. In the numerical analysis, one super inclusion corner element and 508 four-node quadrilateral elements are adopted.

In a word, comparisons aforementioned show that the present *ad hoc* hybrid-stress finite element procedure yields rapidly converging numerical solutions with higher accuracies and fewer elements.
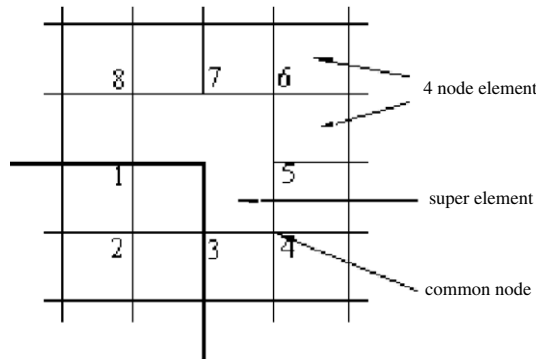


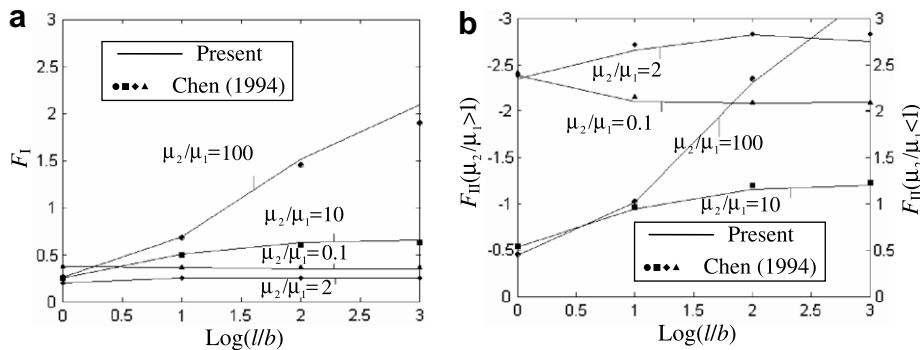**Fig. 6.** Configuration of mesh division around a rectangular corner.



**Fig. 7.** Relationships between $F_{I,\lambda_1}$, $F_{II,\lambda_2}$ and $l/b$ at corner A shown in Fig. 7(a).under tension loading.
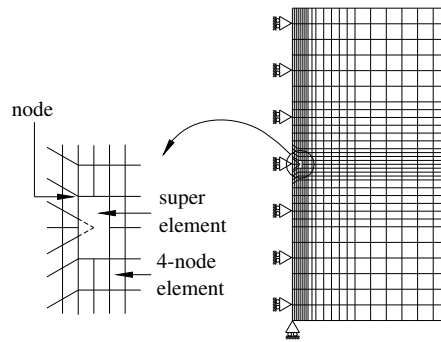
**Fig. 8.** Diagram of finite element mesh division for a diamond inclusion.

**Table 3**
Comparison of dimensionless stress intensity factors $F_{I,\lambda_1}$ and $F_{II,\lambda_2}$ with Chen's (1994)

| Angle $\gamma$ | $\mu_2/\mu_1$ | $F_{I,\lambda_1}(\sigma_y^\infty)$ | | $F_{I,\lambda_1}(\sigma_x^\infty \cap \sigma_y^\infty)$ | | $F_{II,\lambda_2}(\sigma_{xy}^\infty)$ | |
|---|---|---|---|---|---|---|---|
| | | Present | Error | Present | Error | Present | Error |
| 60° | 0.0001 | 1.148 | 0.17 | 1.031 | −0.19 | 1.595 | −0.44 |
| | 0.1 | 0.713 | 0.42 | 0.651 | −0.46 | 1.499 | −0.20 |
| | 10 | −0.106 | 2.91 | 0.311 | −2.20 | – | – |
| | 10000 | −0.111 | −0.89 | 0.349 | −1.69 | −0.556 | −1.07 |
| 120° | 0.0001 | 1.462 | −0.14 | 1.044 | −0.57 | 1.627 | −0.49 |
| | 0.1 | 1.048 | −0.47 | 0.637 | −1.09 | 1.511 | −0.40 |
| | 10 | −0.006 | – | 0.312 | −0.64 | – | – |
| | 10000 | −0.012 | 0.00 | 0.355 | 0.28 | −0.545 | −1.80 |

## 5.3. Numerical results and discussions

### 5.3.1. Interaction between two square isotropic inclusions in isotropic materials

For many heterogeneous materials, the inclusion phases often exhibit irregularities in geometry and randomness in distribution. Therefore, the knowledge of multiple inclusion interactions is very important in evaluating the strength of materials. As an application, an infinite isotropic plate containing two square isotropic inclusions is considered under remote loadings as shown in Fig. 9. The plane strain condition is assumed. The singular stress fields around the inclusion corner o is analyzed. To simulate the infinite effect, the width and the height of the plate are set to be $w = 20b$ and $h = 20b$, respectively, where $b$ is half the width of the square inclusion. Due to the symmetry of the geometry and loading, in the numerical calculations, only one-quarter of the geometry in Fig. 9, i.e., one-quarter of $20b \times 20b$, is needed for finite element mesh division. The numerical solutions of the dimensionless generalized stress intensity factors $F_{I,\lambda_1}$ and $F_{II,\lambda_2}$ under only tension loading $\sigma_{yy}^\infty$ are computed and listed in Table 4. From the Table 4 it can be seen that, as $\mu_2/\mu_1 < 1$, the numerical results of $F_{I,\lambda_1}$ and $F_{II,\lambda_2}$ decrease with the increase of the space distance $d$ between the two square inclusions and they are all greater than zero, implying that both tension fracture and shear fracture might occur at the inclusion corner but shear-oriented fracture might occur; as $\mu_2/\mu_1 > 1$, $F_{I,\lambda_1}$ increases with the increase of the space distance $d$ and is greater than zero, while $F_{II,\lambda_2}$ varies irreg-
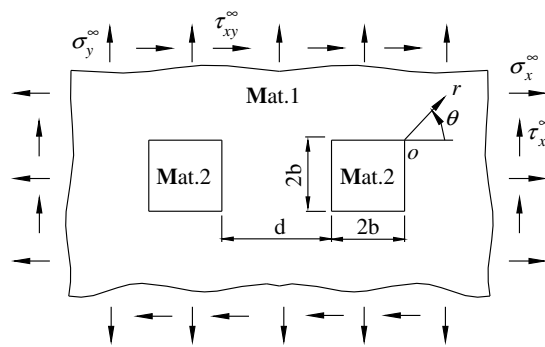


**Fig. 9.** Double square inclusions in an infinite plate.

**Table 4**
Dimensionless GSIFs $F_{I,\lambda_1}$ and $F_{II,\lambda_2}$ around the corner o in Fig. 9 under tension loading $\sigma_{yy}^\infty$

| $d/b$ | SIFs | $\mu_2/\mu_1$ | | | |
|-------|------|------|------|------|------|
| | | 0.1 | 2 | 10 | 100 |
| 0.2 | $F_{I,\lambda_1}$ | 0.4494 | 0.1888 | 0.2075 | 0.2090 |
| | $F_{II,\lambda_2}$ | 2.6723 | −2.3365 | −0.4886 | −0.2971 |
| 0.4 | $F_{I,\lambda_1}$ | 0.4309 | 0.1904 | 0.2104 | 0.2118 |
| | $F_{II,\lambda_2}$ | 2.6094 | −2.3418 | −0.4878 | −0.2965 |
| 0.6 | $F_{I,\lambda_1}$ | 0.4201 | 0.1919 | 0.2135 | 0.2150 |
| | $F_{II,\lambda_2}$ | 2.5711 | −2.3448 | −0.4868 | −0.2959 |
| 0.8 | $F_{I,\lambda_1}$ | 0.4131 | 0.1932 | 0.2165 | 0.2180 |
| | $F_{II,\lambda_2}$ | 2.5450 | −2.3464 | −0.4859 | −0.2952 |
| 1.0 | $F_{I,\lambda_1}$ | 0.4082 | 0.1942 | 0.2191 | 0.2206 |
| | $F_{II,\lambda_2}$ | 2.5261 | −2.3474 | −0.4850 | −0.2947 |

ularly with increasing $d$ and is always less than zero, implying that both tension and shear fracture might occur at the inclusion corner but the shear fracture direction is opposite to that of $\mu_2/\mu_1 < 1$. In addition, with increasing $\mu_2/\mu_1$ ratio, the dimensionless generalized stress intensity factors $F_{I,\lambda_1}$ and $F_{II,\lambda_2}$ are affected by only the space distance $d$ regardless of $\mu_2/\mu_1$ and finally both tension and shear fracture might occur simultaneously. In the numerical computation, two super inclusion corner element and 504 four-node quadrilateral elements are used.

### 5.3.2. A single rectangular isotropic inclusion in composite materials

In this part, as shown in Fig. 5(a), an infinite anisotropic plate containing a single rectangular isotropic inclusion is considered under tension loading. Suppose that domain $\Omega^1$ is occupied by a high modulus epoxy-matrix composite material, and domain $\Omega^2$ by an isotropic material which may be lead (Pb), aluminum (Al), copper (Cu), nickel (Ni) and ceramics (Al$_2$O$_3$). The singular stress fields around the inclusion corner A are analyzed. To simulate the infinite effect, the width and the height of the plate are set to be $w = 20b$ and $h = 10l$, respectively. Diagram of mesh division around the rectangular inclusion corner is given in Fig. 6. Under tension loading $\sigma_{yy}^\infty$, the generalized stress intensity factors GSIFs $K_1$ and $K_2$ near corner A, with varying $l/b$, along the interface AB ($\theta_0 = 3\pi/4$, see Fig. 4) between the matrix and the inclusion are plotted in Fig. 10. We can see from the Figure that, as $l/b < 10$, the GSIFs $K_1$ and $K_2$ for the copper and the ceramics inclusions vary quickly but slowly for the lead and the aluminum inclusions, implying that the higher the modulus of the inclusion is, the greater the effect of the size $l/b$ on the GSIFs $K_1$ and $K_2$ is. As $l/b > 10$, the effect disappears basically. In other words, the inclusion will strengthen the interface, and the higher the modulus of the inclusion is, the stronger the interface is.

### 5.3.3. A single rectangular piezoelectric inclusion in isotropic materials

In the field of intelligent structures, as sensors and actuators, piezoelectric materials are usually embedded or bonded on a host material. As a mechanical model, these cases can be considered as a problem of an infinite plate containing a piezoelectric inclusion. In the present paper, the geometrical configuration of the inclusion is rectangular. Therefore, the problem can be described by Fig. 5(a). Suppose that domain $\Omega^1$ is occupied by an isotropic elastic material (metal) such as aluminum or nickel, and domain $\Omega^2$ by an piezoelectric material such as PZT5H. The singular stress fields around the inclusion corner A
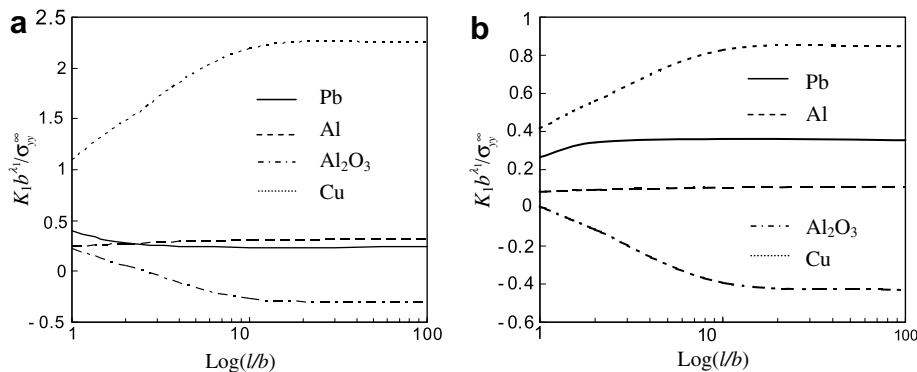


**Fig. 10.** The GSIFs $K_1 b^{\lambda_1}/\sigma_{yy}^\infty$ and $K_2 b^{\lambda_1}/\sigma_{yy}^\infty$ around corner A on interface AB of rectangular inclusion under tension $\sigma_{yy}^\infty$ vs. $l/b$.

**Table 5**
Comparisons of present results and ANSYS solutions of GSIFs for a single rectangular PZT4 inclusion in an aluminum matrix

| $l/b$ | $K_1 b^{\lambda_1}/\sigma_{yy}^{\infty}$ | | | $K_2 b^{\lambda_1}/\sigma_{yy}^{\infty}$ | | |
|---|---|---|---|---|---|---|
| | Present | ANSYS | Errors | Present | ANSYS | Errors |
| 1 | 1.4018 (222) | 1.5227 (4906) | −8.62% | 1.6134 | 1.773 | −9.89% |
| 3.162 | 1.3275 (327) | 1.4430 (6306) | −8.70% | 1.0282 | 1.134 | −10.29% |
| 10 | 1.2659 (372) | 1.3873 (15446) | −9.59% | 1.0016 | 1.1091 | −10.73% |
| 31.62 | 1.2593 (507) | 1.3411 (16274) | −6.50% | 0.9912 | 1.0954 | −10.51% |
| 100 | 1.2535 (507) | 1.3326 (17328) | −6.31% | 0.9821 | 1.0933 | −11.32% |

**Table 6**
Comparisons of present results and ANSYS solutions of GSIFs for a single rectangular PZT5H inclusion in an aluminum matrix

| $l/b$ | $K_1 b^{\lambda_1}/\sigma_{yy}^{\infty}$ | | | $K_2 b^{\lambda_1}/\sigma_{yy}^{\infty}$ | | |
|---|---|---|---|---|---|---|
| | Present | ANSYS | Errors | Present | ANSYS | Errors |
| 1 | 1.6702 (222) | 1.773 (4906) | −6.15% | 0.3995 | 0.3508 | 12.19% |
| 3.162 | 1.2677 (327) | 1.1335 (6306) | 10.59% | 0.2231 | 0.1962 | 12.06% |
| 10 | 1.1926 (372) | 1.1091 (15446) | 7.00% | 0.2057 | 0.18 | 12.49% |
| 31.62 | 1.1339 (507) | 1.0954 (16274) | 3.40% | 0.1815 | 0.17 | 6.34% |
| 100 | 1.1136 (507) | 1.0933 (17328) | 1.82% | 0.179 | 0.163 | 8.94% |

are analyzed. The plane strain condition is assumed. The finite element mesh division is the same as that of the proceeding section. Electric potentials inside the metal and on the interface are assumed to be zero. Under tension loading, the generalized stress intensity factors $K_1$ and $K_2$ near corner A on the interface of $\theta_0 = 3\pi/4$ (see Fig. 4) are calculated and listed in Tables 5 and 6. It can be seen from the Tables that both of $K_1$ and $K_2$ decrease with increasing log($l/b$). In addition, to validate the efficacy of present method, the numerical solutions of $K_1$ and $K_2$ from the commercial software ANSYS are also given in the Tables. Comparisons of our present results with the solutions from ANSYS show that the present results are basically satisfactory. Maximum error of both results is less than 13%. It should be noted that we are herein not going to discuss further the effect of the number of elements used in the calculations on the computational results due to the limited space and the laborious time. Note the figures in the parenthesis in the Tables are the number of elements used in the numerical solutions, which shows much fewer elements are used in the present method.

## 6. Conclusions

In this paper, a new *ad hoc* hybrid-stress finite element is presented for the mechanical analysis of heterogeneous materials with elastic matrix and elastic inclusions. A super $n$-sided polygonal element embedded with a part of an elastic inclusion corner is developed. The present method is validated by comparing its predictions with available numerical solutions of problems with one isotropic rectangular or diamond inclusion in the infinite (large enough) isotropic plate. The analytical singular stress distribution surrounding the inclusion corner is reproduced based on the developed method. Excellent agreement is obtained. Versatility and applicability of the developed method are also demonstrated by examining the effect of material type, stiffness ratio, shape and spacing position on the generalized stress intensity factors (GSIF) around the inclusion corner.

Through our numerical analyses, some useful conclusions can be drawn as follows:

(1) The inclusion will strengthen the interface, and the higher the modulus of the inclusion is, the stronger the interface is.
(2) For the interaction problems of two rectangular inclusions in an isotropic material-matrix under tension loading, the numerical results of $F_{I,\lambda_1}$ and $F_{II,\lambda_2}$ decrease with the increase of the space distance $d$ between the two square inclusions and shear-oriented fracture might occur as $\mu_2/\mu_1 < 1$; the GSIF $F_{I,\lambda_1}$ and $F_{II,\lambda_2}$ are affected only by the space distance $d$ regardless of tension loading and finally both tension and shear fracture might occur simultaneously as $\mu_2/\mu_1 > 10$.
(3) For single rectangular inclusion problems, when $l/b > 10$, the effect of $l/b$ on the generalized intensity factors can be ignored and then the rectangular inclusion can be considered as a fiber.
(4) For inclusions in an anisotropic material-matrix, the effect of inclusion on the generalized intensity factors is very complicated and it needs to be discussed further.

## Acknowledgements

# References

Budiansky, B., 1965. On the elastic moduli of some heterogeneous materials. Journal of the Mechanics and Physics of Solids 13, 223.

Buryachenko, V.A., 2007. Micromechanics of Heterogeneous Materials. Springer, NY.

Buryachenko, V.A., Bechel, V.T., 2000. A series solution of the volume integral equation for multiple inclusion interaction problems. Composites Science and Technology 60, 2465–2469.

Chen, D.H., 1994. Analysis of singular stress field around the inclusion corner tip. Engineering Fracture Mechanics 49, 533–546.

Chen, D.H., Nisitani, H., 1993. Singular stress near the corner of jointed dissimilar materials. Journal of Applied. Mechanics 60, 607–613.

Chen, M.C., Ping, X.C., 2007a. Finite element analysis of piezoelectric corner configurations and cracks accounting for different electric permeabilities. Engineering Fracture Mechanics 74, 1151–1524.

Chen, M.C., Ping, X.C., 2007b. A novel hybrid element analysis for piezoelectric-parent material wedges. Computational Mechanics 40, 13–24.

Chen, M.C., Sze, K.Y., Wang, H.T., 2001a. Analysis of singular stresses in bonded material wedges by computed eigensolutions and hybrid element method. Communications in Numerical Methods in Engineering 17, 495–507.

Chen, M.C., Sze, K.Y., 2001b. A novel hybrid finite element analysis of bimaterial wedge problems. Engineering Fracture Mechanics 68, 1463–1476.

Chen, M.C., Zhu, J.J., Ping, X.C., 2006. Electroelastic singularities in piezoelectric-elastic wedges and junctions. Engineering Fracture Mechanics 73, 855–868.

Dong, C.Y., Bonnet, M., 2002. An integral formulation for steady-state elastoplastic contact over a coated half plane. Computational Mechanics 28, 105–121.

Dong, C.Y., Cheung, Y.K., Lo, S.H., 2002. A regularized domain integral formulation for inclusion problems of various shapes by equivalent inclusion method. Computer Methods in Applied Mechanics and Engineering 191, 3411–3421.

Dong, C.Y., Lo, S.H., Cheung, Y.K., 2003. Stress analysis of inclusion problems of various shapes in an infinite anisotropic elastic medium. Computer Methods in Applied Mechanics and Engineering 192, 683–696.

Eshelby, J.D., 1957. The determination of the elastic field of an ellipsoidal inclusion and related problems. Proceeding of the Royal Society of London A241, 376–396.

Ghosh, S., Mukhopadhyay, S.N., 1993. A material based finite element analysis of heterogeneous media involving Dirichlet tessellations. Computer Methods in Applied Mechanics and Engineering 104, 211–247.

Hill, J.R., 1965. A self consistent mechanics of composite materials. Journal of Mechanics and Physics of Solids 13, 213–222.

Kröner, E., 1958. Berechnung der elastischen Kongstanten des Vielkristalls aus den Kongstanten des Einkristalls. Zeitschrift für Physik 151, 504–518.

Kushch, V.I., Shmegera, S.V., Buryachenko, V.A., 2005. Interacting elliptic inclusions by the method of complex potentials. International Journal of Solids and Structures 42, 5491–5512.

Lee, J., Choi, S., Mal, A., 2001. Stress analysis of an unbounded elastic solid with orthotropic inclusions and voids using a new integral equation technique. International Journal of Solids and Structures 38, 2789–2802.

Lee, J., Gao, H., 1995. A hybrid finite element analysis of interface cracks. International Journal for Numerical Methods in Engineering 38, 2465–2482.

Mori, T., Tanaka, K., 1973. Average stress in matrix and average elastic energy of materials with misfitting inclusions. Acta Metallurgica 21, 571–574.

Moriya, K., 1984. Finite element analysis of stress concentration around elliptic holes, fillets and cracks in plates under stretching and out-of-plane bending. Bulletin of the JSME 27 (234), 2611–2618.

Mura, T., 1987. Micromechanics of Defects in Solids. Martinus Nijhoff Publishers, Dordrecht.

Nakamura, T., Suresh, S., 1993. Effects of thermal residual stresses and fiber packing on deformation of metal-matrix composites. Acta Metallurgica et Materialia 41, 1665–1681.

Nakasone, Y., Nishiyama, H., Nojiri, T., 2000. Numerical equivalent inclusion method: a new computational method for analyzing stress fields in and around inclusions of various shapes. Materials Science and Engineering A285, 229–238.

Nemat-Nasser, S., Muneo, H., 1999. Micromechanics: Overall Properties of Heterogeneous Materials. Elsevier, Amsterdam.

Noda, A.K., Takase, Y., Chen, M.C., 2000. Generalized stress intensity factors in the interaction between two fibers in matrix. International Journal of Fracture 103, 19–39.

Tan, C.L., Gao, Y.L., Afagh, F.F., 1992. Anisotropic stress analysis of inclusion problems using the boundary integral equation method. Journal of Strain Analysis 27, 67–76.

Pian, T.H.H., 1964. Derivation of element stiffness matrices by assumed stress distributions. AIAA Journal 2, 1333–1336.

Sze, K.Y., Wang, H.T., 2000. A simple finite element formulation for computing stress singularities at bimaterial interfaces. Finite Element in Analysis and Design 35, 97–118.

Sze, K.Y., Wang, H.T., Fan, H., 2001. A finite element approach for computing edge singularities in piezoelectric materials. International Journal of Solids and Structures 38, 9233–9252.

Thomson, R.D., Hancock, J.W., 1984. Local stress and strain fields near a spherical elastic inclusion in a physically deforming matrix. International Journal of Fracture 24, 209–228.

Tong, P., 1977. A hybrid crack element for rectilinear anisotropic material. International Journal for Numerical Methods in Engineering 11, 377–403.

Tong, P., Pian, T.H.H., Lasry, S.J., 1973. A hybrid-element approach to crack problems in plane elasticity. International Journal for Numerical Methods in Engineering 7, 297–308.

Wang, X.W., Zhou, Y., Zhou, W.L., 2004. A novel hybrid finite element with a hole for analysis of plane piezoelectric medium with defects. International Journal of Solids and Structures 41, 7111–7128.

Zhang, J., Katusbe, N., 1995. A hybrid finite element method for heterogeneous materials with randomly dispersed elastic inclusions. Finite Element in Analysis and Design 19, 45–55.

Zhang, J., Katusbe, N., 1997. A hybrid finite element method for heterogeneous materials with randomly dispersed rigid inclusions. Computer Methods in Applied Mechanics and Engineering 148, 225–234.